Journal of Applied Polymer Science

Effects of Melt Structure on Crystallization Behavior of Isotactic Polypropylene Nucleated with α/β Compounded Nucleating Agents

Qiyan Zhang,[1,2,3] Zhengfang Chen,[1,2] Bing Wang,[1,2] Jinyao Chen,[1,2] Feng Yang,[1,2] Jian Kang,[1,2] Ya Cao,[1,2] Ming Xiang,[1,2] Huilin Li[1,2]

[1]State Key Laboratory of Polymer Materials Engineering, Chengdu 610065, People's Republic of China
[2]Polymer Research Institute of Sichuan University, Chengdu 610065, People's Republic of China
[3]College of Polymer Science & Engineering of Sichuan University, Chengdu 610065, People's Republic of China
Correspondence to: J. Kang (E-mail: jiankang@scu.edu.cn) and Y. Cao (E-mail: caoya@scu.edu.cn)

ABSTRACT: In this study, the melt structure of isotactic polypropylene (iPP) nucleated with α/β compounded nucleating agents (α/β-CNA, composed of the α-NA of 0.15 wt % Millad 3988 and the β-NA of 0.05 wt % WBG-II) was tuned by changing the fusion temperature T_f. In this way, the role of melt structure on the crystallization behavior and polymorphic composition of iPP were investigated by differential scanning calorimetry (DSC), wide-angle X-ray scattering (WAXD) and scanning electron microscopy (SEM). The results showed that when $T_f = 200°C$ (iPP was fully molten), the α/β-CNA cannot encourage β-phase crystallization since the nucleation efficiency (NE) of the α-NA 3988 was obviously higher than that of the β-NA WBG-II. Surprisingly, when T_f was in 179–167°C, an amount of ordered structures survived in the melt, resulting in significant increase of the proportion of β-phase (achieving 74.9% at maximum), indicating that the ordered structures of iPP played determining role in β-phase crystallization of iPP nucleated with the α/β-CNA. Further investigation on iPP respectively nucleated with individual 3988 and WBG-II showed that as T_f decreased from 200°C to 167°C, the crystallization peak temperature T_c of iPP/3988 stayed almost constant, while T_c of iPP/WBG-II increased gradually when $T_f < 189°C$ and became higher than that of iPP/3988 when T_f decreased to 179°C and lower, which can be used to explain the influence of ordered structure and α/β-CNA on iPP crystallization. Using this method, the selection of α-NA for α/β-CNA can be greatly expanded even if the inherent NE of β-NA is lower than that of the α-NA. © 2014 Wiley Periodicals, Inc. J. Appl. Polym. Sci. **2015**, *132*, 41355.

KEYWORDS: crystallization; morphology; polyolefins; thermal properties

Received 24 May 2014; accepted 27 July 2014
DOI: 10.1002/app.41355

INTRODUCTION

As one of the most widely used semi-crystalline polymers,[1–7] isotactic polypropylene (iPP) exhibits a very interesting polymorphic behavior, sharing at least four crystalline structures: monoclinic α-form,[8–10] trigonal β-form,[11–14] triclinic γ-form,[15,16] and smectic phase.[17–21] Among these crystalline forms, the α-form is the most common and stable modification, being found in most melt-crystallized specimens.[22–24] The β-form is a metastable phase and can only be obtained in large amount under specific processing conditions such as melt crystallization in the presence of specific heterogeneous nucleating agent (NA),[25–30] by directional crystallization in certain temperature,[31] or from melts subject to shear.[32–35] The addition of β-NA is an effective and practical way to obtain high proportion of β-fraction. The γ-form is only found in the case of low-molecular weight iPP and in random copolymers of propylene and α-olefins[16,36] or by the effect of pressure.[37,38] The mechanical properties of iPP are largely related to the crystal structure and morphology, which in turn depends on the crystallization conditions and NAs.

Different specific NAs are usually added to improve the properties of iPP by inducing the special crystal form (α-form or β-form), decreasing the spherulite size and improving the crystallinity during crystallization. So far, at least two kinds of NAs, α- and β-NAs, have been developed.[39,40] The α-NA can improve the stiffness and optical properties of iPP while decrease its ductility, while the β-NA can greatly improve iPP's toughness and ductility while decrease its stiffness. Thereby, it is well expected to balance the stiffness and toughness of iPP using the α/β compounded NAs (denoted as α/β-CNA in this study). Xin's research group[41,42] proposed an idea of compounding the β- and α-NAs and claimed that α/β-CNA will not only realize balance adjustment of toughness and stiffness of iPP but also shorten molding cycle time of iPP obviously; Bai et al.[42–44] studied the isothermal and non-isothermal crystallization

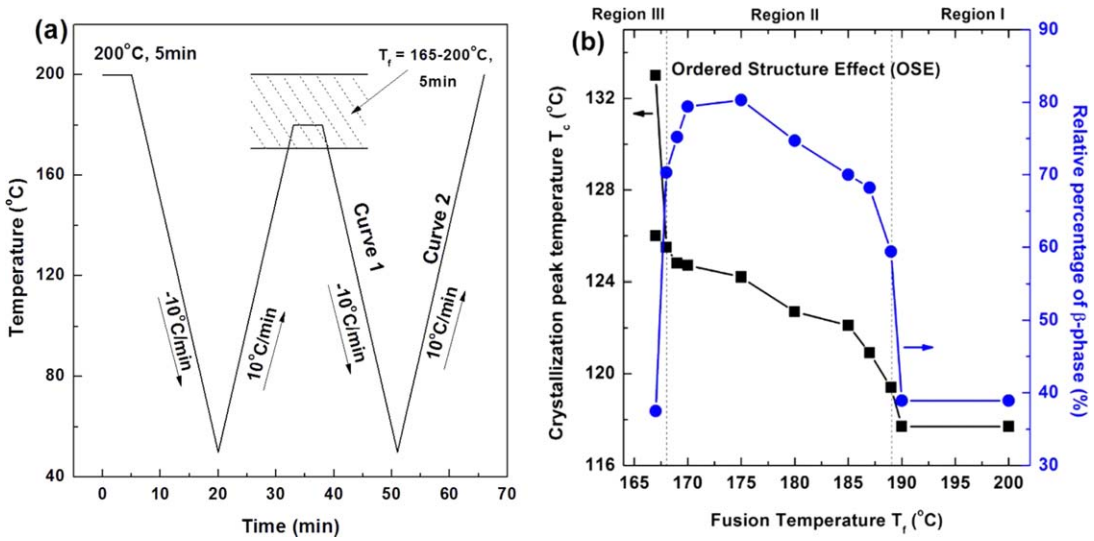

Scheme 1. (a) Schematic illustration of the thermal treatment protocol to study the crystallization and melting behavior of iPP with different melt structures and (b) Variations of crystallization peak temperature (T_c) and the relative percentage of β-phase (β_c) as a function of the fusion temperature (T_f) of iPP nucleated with the dual-selective β-NA (rare earth based β-NA WBG-II, concentration 0.03 wt %). [Color figure can be viewed in the online issue, which is available at wileyonlinelibrary.com.]

behavior of iPP nucleated by α/β-CNA; Zhao et al.[39] investigated the nucleation characteristic of α/β-NA during the crystallization process of iPP and proposed the principle determining the polymorphic behavior of the sample: the NA with higher nucleation efficiency (NE, the relative increment of crystallization peak temperature induced by the NA) played a leading role in determine the final crystalline form of iPP nucleated with α/β-NA. If the NE of α-NA was higher than that of the β-NA, the β-phase can hardly be obtained when these two NAs are compounded; considering the restrict of this principle, the selection of α- and β-NAs for the α/β-CNA is very limited.

On the other hand, it was found that if the fusion temperature (heating temperature, T_f) was not high enough to make the polymer fully molten, an amount of ordered structures would survive within the melt and provide unsurpassed NE for the crystallization process, which was call the self-nucleation.[45–53] Although the physical nature of the ordered structures are still under debate,[45,52] it is well accepted that the presence of ordered structures can accelerate crystallization rate and elevated the crystallization temperature of the polymer.

More interestingly, recent studies pointed out that the ordered structures are crucial to the β-phase crystallization of iPP. Yan et al.[33–35,54] introduced partly melting iPP fiber to homogeneous supercooled iPP melt and claimed that the partly melting of orientated ordered structure derived from the iPP fiber played very important role in the β-nucleation. Alfonso et al.[55–57] found that shear flow and partially molten fiber had similar effect on the formation of β-phase. Shen et al.[32,58] studied the crystallization of iPP ordered melt under low shearing stress and found that only in the presence of ordered structures can the sheared iPP melt form the β-crystals.

Recently, our group[59] tuned the T_f as described in Scheme 1(a) to control the melt structure of iPP (i.e., to control content of ordered structures in iPP melt). In this way, the role of melt structure in β-phase crystallization of iPP nucleated with various representative NAs were studied. We surprisingly found that for iPP nucleated with α-/β-dual selective β-NA (dual-selective β-NA, such as the rare earth based β-NA, WBG-II, and the widely used *N,N′*-dicyclohexyl-2,6-naphthalenedicarboxamide, DCNDCA), the melt structure of iPP played very important role in the β-crystallization process. When T_f was proper for the melt to preserve an amount of ordered structures, these ordered structures exhibited high β-NE under the influence of dual-selective β-NA, resulting in the elevated crystallization temperature (i.e., evident increase of NE) and significant increase of the relative percentage of β-phase [Scheme 1(b)], which was called as the ordered structure effect (OSE). In another study,[60] we explored the roles of the cooling rates and the end temperature of recooling in the occurrence of the OSE behavior.

As was illustrated in Scheme 1(b), according to the variations of crystallization peak temperature on the DSC cooling curves (T_c) and the relative percentage of β-phase on the DSC heating curves (β_c), the temperature range of T_f was divided into three regions, Regions-I, -II, and -III: (i) When T_f was higher than 189°C, the complete melting was achieved (i.e., no ordered structures survived in the melt), and the constant T_c and β_c were observed. The corresponding T_f temperature range was defined as Region I (T_f, 189°C in the study); (ii) when T_f was in the temperature range of 168–189°C, the ordered structures exhibited high β-NE under the influence of the dual-selective β-NA and evidently increased the T_c and β_c, which was called the OSE. The corresponding T_f temperature range of 168–189°C was denoted as Region II; when T_f decreased to lower than 168°C, the OSE disappeared due to the existence of the survived α-ordered entities, which can induce annealing and α-recrystallization and thus apply a negative effect on the β-crystallization. A second crystallization peak emerged at high

temperature range and the β_c decreased significantly. The corresponding T_f range was named as Region III (T_f lower than168°C). The results above elucidated first evidence that for iPP nucleated with dual-selective β-NA, the presence of ordered structures in iPP melt plays very important role. Moreover, considering the previous reports concerning the role of ordered structures under shearing or orientation in β-crystallization of iPP[32–35] as well as the studies focusing the β-crystallization behavior of iPP induced by dual-selective β-NAs,[61,62] our findings provided a very important speculation: under all the crystallization conditions mentioned above, the β-nucleation mechanism might be similar, where ordered structures play a determining role. A possible mechanism depicting a two-step β-nucleation behavior of iPP had been proposed in the previous studies.

As mentioned above, the inherent NE of the individual α- and β-NA plays very important role in the compounding of α/β-CNA, meanwhile, the NE of dual-selective β-NA can be efficiently enhanced by creating the ordered structures in iPP melt, which provides an opportunity that for the α/β-CNA including dual-selective β-NA, the selection of the α-NA can be greatly expanded by creating the ordered structures (i.e., controlling the melt structures) in the iPP melt; using this novel method, the polymorphic behavior and the morphology of iPP nucleated with α/β-CNA is expected to be efficiently controlled, which is of great importance in both scientific and practical aspects.

This study aims to explore the influence of melt structure and α/β-CNA on crystallization behavior of iPP. The NE and proportion of β-phase of iPP samples nucleated with the individual β- or α-NA were also studied in order to elucidate the related principle.

EXPERIMENTAL

Materials

iPP, tradename T38F (Lanzhou OilChem, China) with average isotacticity 97.6%, weight average molecular weight 3,47,200, polydispersity index = 3.63, was used.

The β-NA (tradename WBG-II) was supplied by Guangdong Winner Functional Materials, China. WBG-II is heteronuclear dimetal complex of lanthanum and calcium with some specific ligands, which is a kind of irregular block-like crystal whose single crystal diameters is about tens of nanometers. WBG-II has a general formula of $Ca_xLa_{1-x}(LIG1)_m(LIG2)_n$, where x and $1-x$ is the proportion of Ca^{2+} and La^{3+} ion in the complex, while LIG1 and LIG2 are, respectively, a dicarboxylic acid and amide-type ligand with coordination numbers of m and n.

The α-NA was widely used 1,3 : 2,4-bis (3,4-dimethylobenzylideno) sorbitol (DMDBS, tradename Millad 3988), supplied by Milliken Chemical, Belgium. The chemical structure of DMDBS can be seen from Figure 1.

Sample Preparation

The iPP pellets and α- or β-NA were individually mixed in the weight ratio of 100 : 1 and then extruded by a twin-screw extruder (SHJ-20, Nanjing Giant Machinery) and pelletized to obtain master batch. The master batch and iPP were mixed and extruded by twin-screw again to obtain the α- and β-iPP with the NA concentrations of 0.15 wt % and 0.05 wt %, respectively. In this way, the iPP nucleated with α/β-CNA was also prepared, where the concentrations of the α- and β-NAs were 0.15 wt % and 0.05 wt %, respectively.

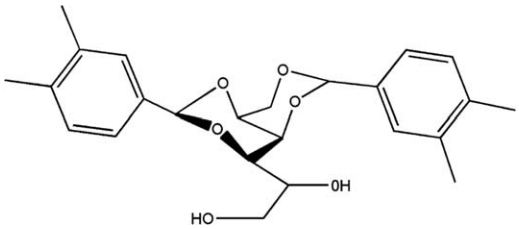

Figure 1. Chemical structure of DMDBS (Millad 3988).

Differential Scanning Calorimetry (DSC)

All the calorimetric experiments were performed with Mettler Toledo DSC1 (Mettler, Switzerland) differential scanning calorimeter (DSC) under nitrogen atmosphere (50 mL/min). The temperature scale calibration was performed using indium as a standard to ensure reliability of the data obtained. 2–5 mg round samples were used. All the thermograms were fitted using Peakfit 4.12 software according to the literature.[3,63] The relative percentage crystallinity of β-crystal (β_c) was estimated by the following expression:

$$\beta_c = X_\beta / (X_\beta + X_\alpha) \quad (1)$$

where the degree of crystallinities X_α and X_β associated with α-phase and β-phase, respectively.

Using the thermal treatment protocol in Scheme 1(a), the content of ordered structures in iPP melt was efficiently controlled. The sample was first heated to 200°C and held for 5min to erase any previous thermal history. Then it was cooled to 50°C at 10°C/min to create "standard" thermal history. After that, it was heated to different fusion temperature (T_f, ranging from 165 to 200°C) at 10°C/min and held for 5 min to create different melt structures. Then, it was cooled down to 50°C at the cooling rate of 10°C/min. Finally, it was heated to 200°C at 10°C/min.

Wide-Angle X-ray Diffraction (WAXD)

WAXD patterns were recorded with a DX-1000 diffractometer. The wavelength of CuKα was $\lambda = 0.154$ nm and the spectra were recorded in the 2θ range of 5–35°, a scanning rate of 2°/min, and a scanning step of 0.02°.

The relative percentage of the β-crystal was determined according to standard procedures described in the literature,[26] employing the following equation:

$$k_\beta = \frac{H_\beta(110)}{H_\beta(110) + H_\alpha(110) + H_\alpha(040) + H_\alpha(130)} \quad (2)$$

where k_β denotes the relative content of β-crystal form (WAXD), $H_\alpha(110)$, $H_\alpha(040)$, and $H_\alpha(130)$ are the intensities of the strongest peaks of α-form attributed to the (110), (040), and (130) planes of monoclinic cell, respectively. $H_\beta(110)$ is the intensity of the strongest (110) diffraction peak of the trigonal β-form.[11,14]

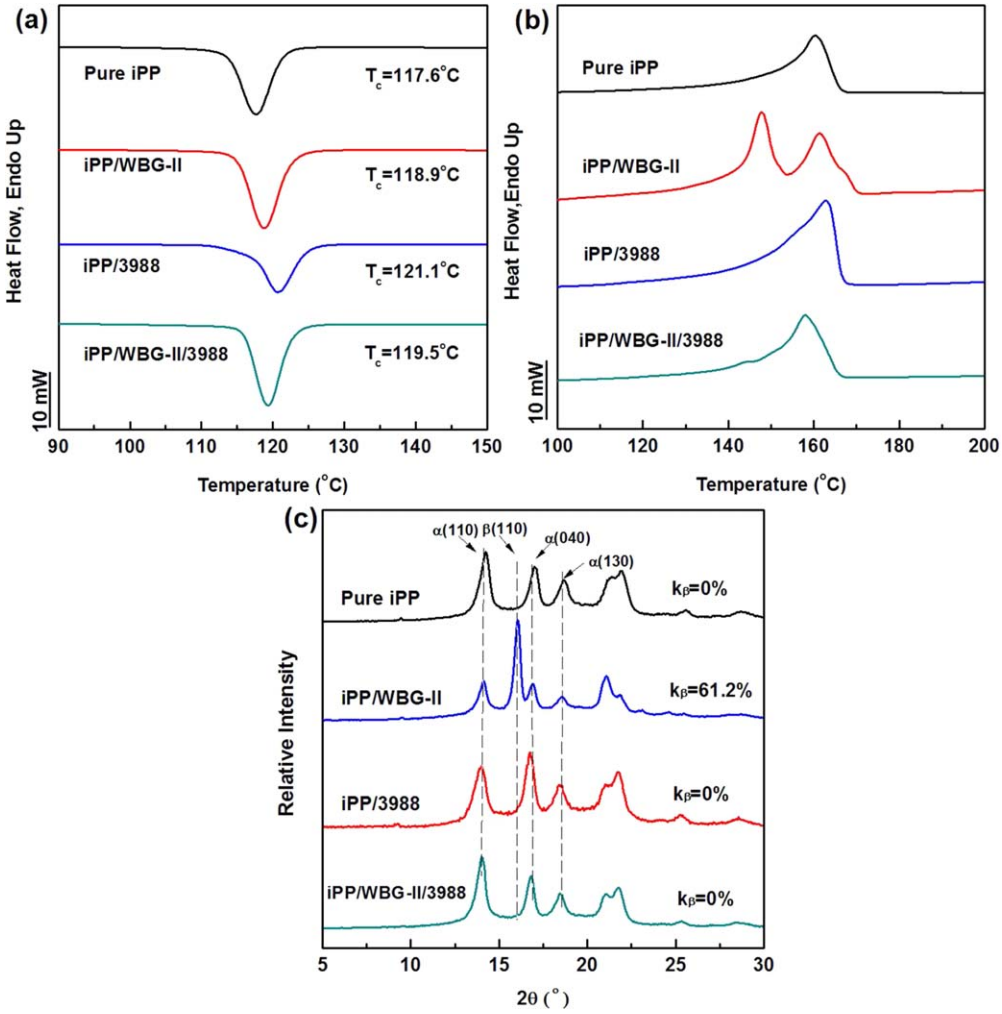

Figure 2. (a) DSC cooling curves and (b) heating curves of pure PP and PP nucleated with 0.05 wt % WBG-II, 0.05 wt % 3988 and WBG-II/3988 (0.05 wt %/0.15 wt %). The cooling and heating rates are 10°C/min. (c) WAXD patterns of the samples. [Color figure can be viewed in the online issue, which is available at wileyonlinelibrary.com.]

Scanning Electron Microscopy (SEM)

The morphology observation (SEM) was performed on a JSM-5900 LV environmental scanning electron microscope (JEOL, Japan) at an accelerating voltage of 20 kV. Before SEM characterizations, the surfaces of all the samples were coated with a thin layer of gold by ion sputtering. All the samples were etched for 2 h in a solution containing 1.3 wt % potassium permanganate ($KMnO_4$), 32.9 wt % concentrated sulfuric acid (H_2SO_4) and 65.8 wt % concentrated phosphoric acid (H_3PO_4), according to the procedure proposed in the References 12 and 64.

RESULTS AND DISCUSSIONS

Crystallization Behavior of the Pure and Nucleated iPP

Nucleation Efficiency Evaluation. The crystallization and melting behaviors of the pure iPP and nucleated iPP are studied by DSC, WAXD. To benefit discussion, iPP nucleated with 0.05 wt % WBG-II, 0.05 wt % 3988 and WBG-II/3988 (0.05 wt %/0.15 wt %) are denoted as iPP/WBG-II, iPP/3988 and iPP/WBG-II/3988, respectively. The DSC cooling and heating curves as well as the WAXD profiles of the samples are plotted in Figure 2.

Figure 2 shows that after the addition of β-NA WBG-II, the crystallization peak temperature T_c of iPP increases and an amount of β-phase forms [as can be seen from the melting peak located at the temperature range of lower than 155°C in Figure 2(b), and the diffraction peak at $2\theta = 16.1^o$, characteristic of $\beta(110)$, in Figure 2(c)], exhibiting high β-NE of the NA; After the addition of the α-NA 3988, the increment of T_c is observed due to the α-NE of the NA; However, after the addition of α/β-CNA of WBG-II/3988, no β-phase forms. To fully understand this, the NE of the individual NAs are evaluated according to the methodology developed by Fillon et al.,[29] employing the following eq. (3):

$$NE = \frac{T_{cNA} - T_{c1}}{T_{c2\,\max} - T_{c1}} \quad (3)$$

where T_{cNA}, T_{c1}, and T are peak crystallization temperatures of the nucleated, non-nucleated and self-nucleated polymer, respectively. The NE is here expressed as a percentage where zero stands for no nucleating action and 100 for optimum efficiency.[51] According to Fillon's assumption, the self-nucleation procedure allows obtaining the highest achievable crystallization

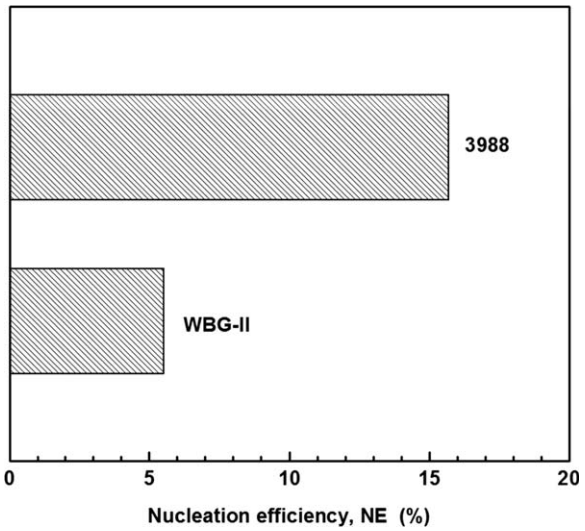

Figure 3. The nucleation efficiencies of iPP nucleated by 0.15 wt % α-NA 3988 and 0.05 wt % β-NA WBG-II, respectively.

temperature. The T_{c2max} of the self-nucleated iPP used in this study is 140°C.[65] The NEs of the individual α- and β-NAs are calculated as shown in Figure 3.

Clearly, the NE of iPP/3988 is evidently higher than that of iPP/WBG-II. According to the principle proposed by Zhao et al.[39] that in the α/β-CNA, the one with higher NE of the individual α- and β-NA determines the final crystalline form of the nucleated iPP, it can be concluded that the α/β-CNA of WBG-II/3988 can only induce α-phase and cannot induce the formation of β-phase in iPP as observed in Figure 1.

Crystallization Behavior of Nucleated iPP with Different Melt Structures

By tuning the fusion temperature T_f, the melt structure status of iPP nucleated with dual-selective β-NA (such as WBG-II) can be controlled, resulting in an evident increase of β-NE of the sample, which brings an opportunity to control the individual NE of WBG-II in the α/β-CNA system and therefore control the final polymorphic behavior of the nucleated iPP. Therefore, in this section the thermal treatment shown in Scheme 1(a) is applied to study the crystallization and melting behavior of the nucleated iPP with different melt structures.

Crystallization Behavior. The obtained cooling curves [Curve 1 in Scheme 1(a)] are shown in Figure 4(a). The variations of crystallization parameters, the peak, onset, and endset crystallization temperatures (T_c, T_{conset}, and $T_{c\ endset}$) are plotted as a function of T_f as shown in Figure 4(b).

As can be seen from Figure 4, when T_f is higher than 179°C, the crystallization temperatures stay almost constant with the variation of T_f, reflecting constant nucleation density of the melt, namely, iPP is fully molten; In the T_f range of 179–167°C, T_c increases gradually with the decrease of T_f, indicating that the fusion temperature is not high enough to make the melt fully molten, leaving an amount of ordered structures in the melt; as T_f decreases to lower than 167°C, the crystallization peak significantly widens and two peaks can be observed, indicating that T_f is so low that the large ordered entities can survive in the melt,[65] which are large enough to induce annealing or recrystallization in the course of subsequent cooling and therefore induce in a second crystallization peak in the high temperature range.

Melting Behaviors. The subsequent heating curves of the sample [Curve 2 in Scheme 1(a)] are recorded as shown in Figure 5(a). The relative percentages of the β-phase (β_c) are calculated and plotted in Figure 5(b) as a function of the fusion temperature T_f.

Interestingly, Figure 5 shows that for iPP nucleated with α/β-CNA, when T_f is higher than 179°C, the sample is fully molten

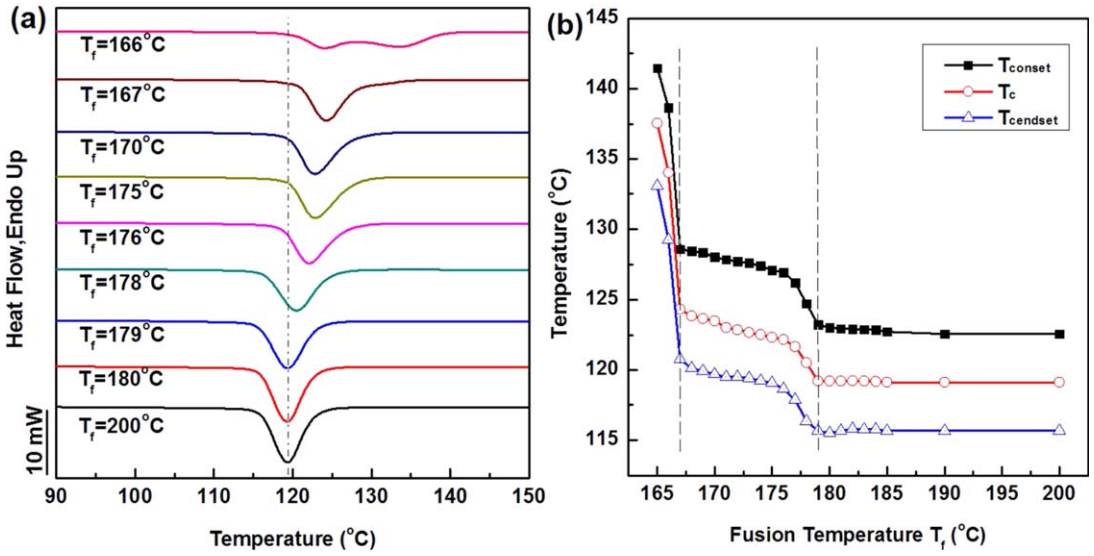

Figure 4. (a) Cooling curves of PP nucleated with α/β-CNA (WBG-II: 3988 = 0.05 wt % : 0.15 wt %) after held at the indicated fusion temperature (T_f, ranging from 165–200°C) for 5 min. (b) Variations of crystallization parameters of the sample, the peak, onset and endset crystallization temperatures (T_c, $T_{c\ onset}$ and $T_{c\ endset}$), as a function of T_f. [Color figure can be viewed in the online issue, which is available at wileyonlinelibrary.com.]

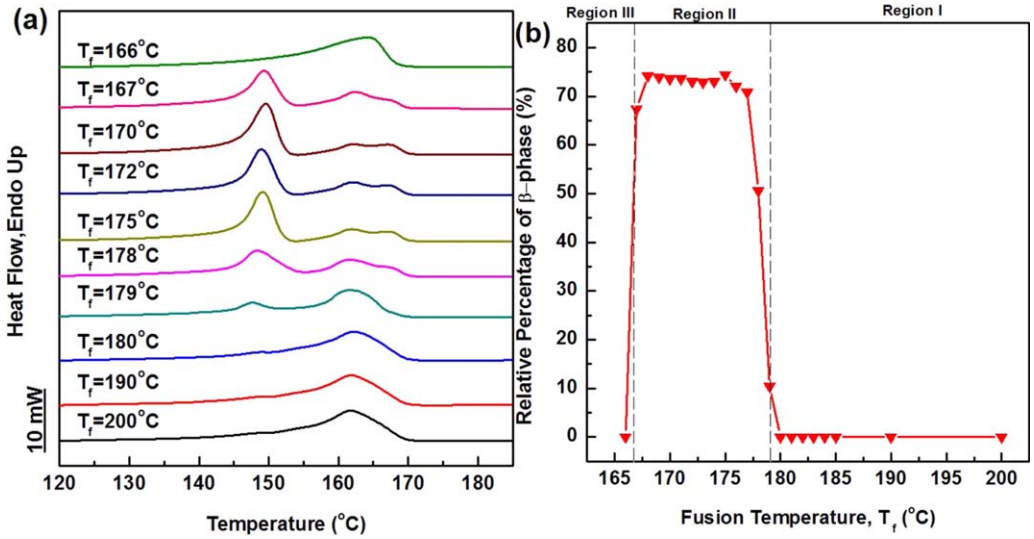

Figure 5. (a) DSC heating curves of iPP nucleated with α/β-CNA (WBG-II: 3988 = 0.05 wt % : 0.15 wt %) after held at T_f for 5 min and then cooled to 50°C at 10/min. (b) Relative percentages of β-phase(β_c) calculated from DSC heating curves. [Color figure can be viewed in the online issue, which is available at wileyonlinelibrary.com.]

and no β-phase has formed due to the relatively low NE of the individual WBG-II compared with that of 3988; surprisingly, when T_f is in the temperature range of 167–179°C, the intensity of the β-melting peak (located at the temperature range of lower than 155°C) increases evidently with the decrease of T_f. The proportion of β-phase (β_c) increases significantly from zero (when T_f, 179°C) to 74.9% at maximum; When T_f is not higher than 167°C, β_c decreases sharply due to the α-nucleation effect of the survived large ordered entities as discussed above. The surprising increment of β_c with the variation of T_f observed above indicates that the polymorphic behavior of iPP nucleated with α/β-CNA is greatly dependent on the T_f, in another word, the content of ordered structures in the melt. There exists a syn-

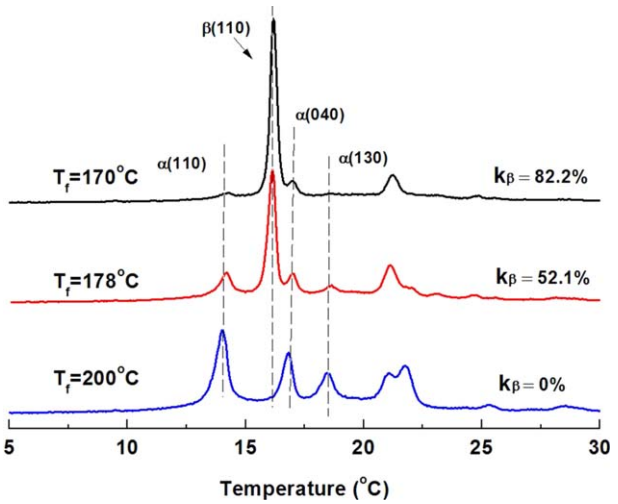

Figure 6. WAXD profiles of iPP nucleated with α/β-CNA (WBG-II: 3988 = 0.05 wt % : 0.15 wt %) after held at T_f for 5 min and then cooled to room temperature at 10°C/min. [Color figure can be viewed in the online issue, which is available at wileyonlinelibrary.com.]

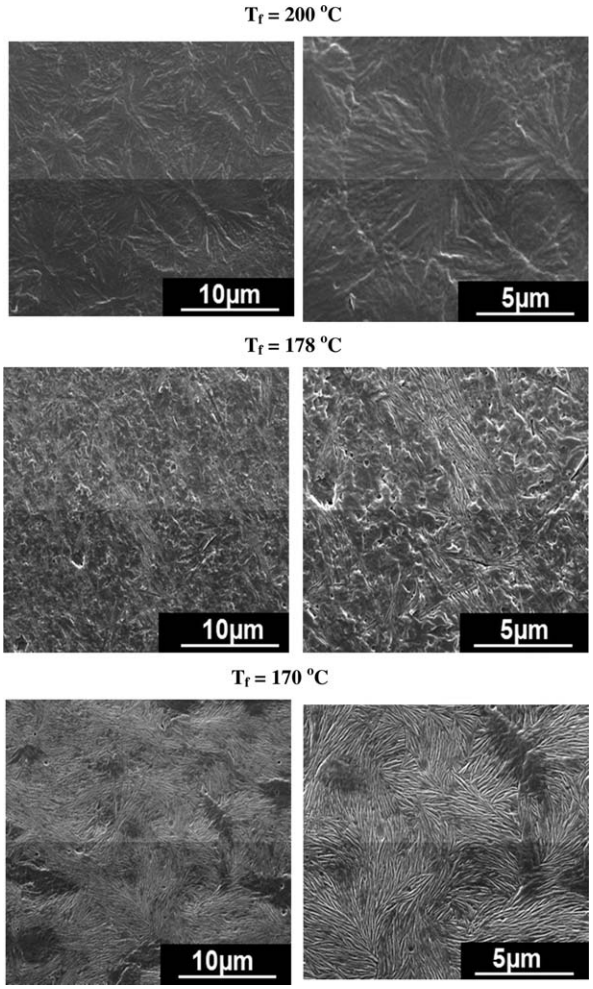

Figure 7. SEM images (after etching) of iPP nucleated with α/β-CNA (WBG-II: 3988 = 0.05 wt % : 0.15 wt %) after held at the indicate fusion temperature (T_f) for 5min and then cooling to room temperature.

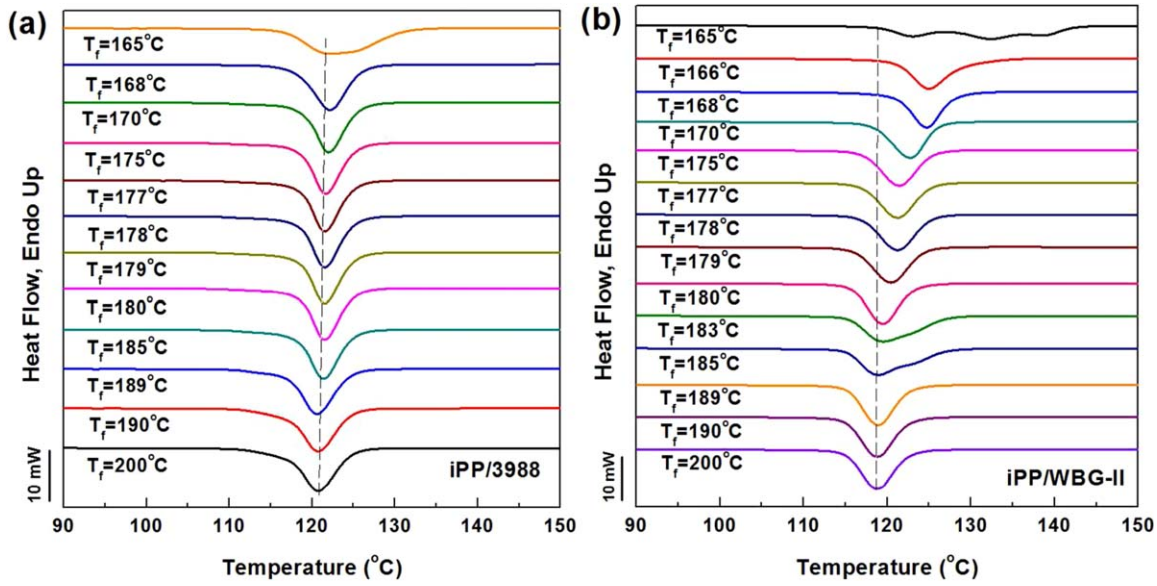

Figure 8. curves of samples after held at the indicated fusion temperature T_f for 5 min (T_f ranges from 165 to 200°C) (a) iPP/3988 (NA concentration 0.15 wt %) (b) iPP/WBG-II (concentration 0.05 wt %). [Color figure can be viewed in the online issue, which is available at wileyonlinelibrary.com.]

ergetic effect between the α/β-CNA (3988/WBG-II) and the ordered structures of iPP, which can evidently increase the β-NE of the sample.

According to the variations of T_c on the cooling curves (Figure 4) and β_c on the heating curves (Figure 5) with the change of T_f, the whole T_f temperature range can be divided in to three regions as indicated by the dotted lines in Figure 5(b):

i. Region I ($T_f > 179$°C in this study), where iPP is fully molten, the nucleation density in the melt is constant, T_c and β_c are constant;
ii. Region II (167°C $\leq T_f \leq$ 179°C), where the iPP is partially melting and an amount of ordered structures survive in the melt. Under the synergetic effect between the α/β-CNA and the ordered structures of iPP, the β-NE of the sample is evidently elevated, which further results in the increase of T_c and β_c;
iii. Region III ($T_f <$ 167°C), where the large ordered entities that can induce annealing or recrystallization during the subsequent cooling can survive in the melt, resulting in emergence of second crystallization peak and the sharp decrease of β_c.

Figure 6 is the WAXD profiles of the sample after held at the representative T_f of 170, 178, and 200°C for 5 min and then cooled to room temperature. In Figure 6, the variation of β-phase content (k_β) with the change of T_f is in accord with the results in Figure 5.

Morphology Observation by SEM. To directly observe the impact of the α/β-CNA and ordered structures on the crystalline morphology of iPP, the SEM morphological observation is performed on the etched samples. The samples are prepared through hot-molding process with different molding temperature (i.e., fusion temperature T_f). The results are shown in Figure 7.

When $T_f = 200$°C, only the dark spherulites with diameter about 20μm can be observed, which are α-spherulites; As T_f comes to 178°C, the spherulite sizes decrease sharply, and both dark and bright crystals can be observed, corresponding to α- and β-phase respectively[65–70]; as the T_f decreases to 170°C, large amount of β-crystals almost fill up the SEM screen, showing the formation of high proportion of β-phase.

Discussions

The above results demonstrate that the ordered structures play an important role in determining the β-crystallization of iPP nucleated with α/β-CNA of WBG-II/3988, although the inherent NE of the β-NA WBG-II is lower than that of the α-NA 3988. In ordered to fully understand the role of ordered structures, in this section we studied the variation of crystallization peak temperature T_c (direct indicator of the nucleation efficiency NE)

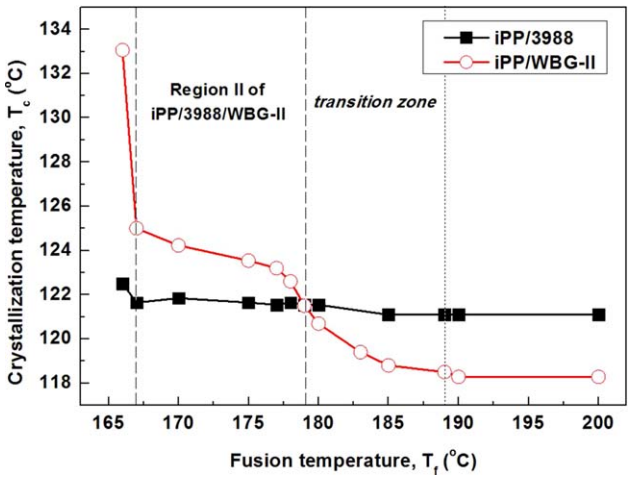

Figure 9. Plots of the crystallization peak temperature T_c of iPP/3988 and iPP/WBG-II as a function of the fusion temperature T_f. [Color figure can be viewed in the online issue, which is available at wileyonlinelibrary.com.]

with the change of fusion temperature T_f of iPP nucleated with 0.15 wt % WBG-II and 0.05 wt % 3988, respectively. The obtained cooling curves of iPP/3988 and iPP/WBG-II after held at the indicated T_f for 5 min are shown in Figure 8. The variations of T_c of the samples are plotted as a function of T_f as shown in Figure 9.

Figures 8 and 9 show that the T_c of iPP/3988 stays almost unchanged as the T_f varies from 200°C to 167°C, indicating that the NE of 3988 cannot be enhanced by tuning the content of ordered structures in iPP. On the other hand, the T_c of iPP/WBG-II increases gradually with the decrease of T_f from 200°C to 167°C, indicating the increase of β-NE of WBG-II. What's more, Figure 9 also reveals a transition zone, T_f = 179–189°C: when T_f decreases to 189°C and lower, T_c starts to increase with the decrease of T_f. Once T_f is 179°C and lower, the T_c of iPP/WBG-II becomes higher than that of iPP/3988. Note that 179°C is the upper limiting temperature of Region II of iPP nucleated with the α/β-CNA of WBG-II/3988. In another word, when T_f is 179°C and lower, the NE of WBG-II becomes higher than that of 3988, resulting in the significant increase of β-phase proportion in the iPP nucleated with the α/β-CNA. In this way, the selection of α-NA for the α/β-CNA can be greatly expanded, even if the inherent NE of the β-NA is lower than that of the α-NA, which is of great importance in the preparation of high-performance polymer products.

CONCLUSIONS

In this study, the melt structure of iPP nucleated with α/β compounded nucleating agents (α/β-CNA including the α-NA of 0.15 wt % Millad 3988 and β-NA of 0.05 wt % WBG-II) was tuned by changing the fusion temperature T_f. The influence of melt structure and α/β-CNA on the crystallization and melting behavior of iPP was investigated by means of DSC, WAXD, and SEM. The conclusions can be drawn as follows:

1. It was observed that the individual NE of the α-NA 3988 was obviously higher than that of the β-NA WBG-II. When these NAs were compounded, the α/β-CNA cannot induce any β-phase crystallization in iPP;
2. By tuning the fusion temperature T_f, the melt structure of iPP (i.e., the content of ordered structures in the melt) was controlled. It was found that the ordered structures played a determining role in the β-crystallization of iPP nucleated with α/β-CNA. When T_f was in the range of 179–167°C, an amount of ordered structures survived in the melt, resulting in a significant increase of the proportion of β-phase, achieving 74.9% at maximum;
3. The variations of crystallization peak temperature T_c with the change of T_f of iPP samples respectively nucleated with individual 3988 and WBG-II were explored. As the T_f decreases from 200°C to 167°C, the T_c of iPP/3988 stayed almost constant, meanwhile, the T_c of iPP/WBG-II increased gradually when T_f decreased to 189°C and became higher than that of iPP/3988 once T_f decreased to 179°C and lower, namely, the NE of WBG-II became higher than 3988 when T_f was in the range of 179–167°C, which can be used to explain the synergetic effect between the ordered structures of iPP and α/β-CNA. Using this method, the selection of α-NA for the α/β-CNA can be greatly expanded even if the inherent NE of the β-NA is lower than that of the α-NA, which is of great importance in the preparation of high-performance polymer products.

ACKNOWLEDGMENTS

The authors gratefully acknowledge the financial support from the Sichuan University Scientific Research Foundation for Young Teachers (2012SCU11075) and National Science Foundation of China (NSFC 51203106) for the financial support.

REFERENCES

1. Du, M.; Guo, B.; Wan, J.; Zou, Q.; Jia, D. *J. Polym. Res.* **2010**, *17*, 109.
2. Kang, J.; Li, J.; Chen, S.; Zhu, S.; Li, H.; Cao, Y.; Yang, F.; Xiang, M. *J. Appl. Polym. Sci.* **2013**, *013*, 25.
3. Kang, J.; Chen, J.; Cao, Y.; Li, H. *Polymer* **2010**, *51*, 249.
4. De Rosa, C.; Auriemma, F. *J. Am. Chem. Soc.* **2006**, *128*, 11024.
5. Kang, J.; Cao, Y.; Li, H.; Li, J.; Chen, S.; Yang, F.; Xiang, M. *J. Polym. Res.* **2012**, *19*, 37.
6. Kang, J.; Yang, F.; Wu, T.; Li, H.; Cao, Y.; Xiang, M. *Eur. Polym. J.* **2012**, *48*, 425.
7. Busico, V.; Cipullo, R. *Prog. Polym. Sci.* **2001**, *26*, 443.
8. Kang, J.; Wang, B.; Peng, H.; Chen, J.; Cao, Y.; Li, H.; Yang, F.; Xiang, M. *Polym. Bull.* **2014**, *71*, 563.
9. Kang, J.; Li, J.; Chen, S.; Peng, H.; Wang, B.; Cao, Y.; Li, H.; Chen, J.; Gai, J.; Yang, F.; Xiang, M. *J. Appl. Polym. Sci.* **2013**, *129*, 2663.
10. Natta, G.; Corradini, P. *Il Nuovo Cimento Series 10* **1960**, *15*, 40.
11. Lotz, B. *Eur. Phys. J.* **2000**, *3*, 185.
12. Peng, H.; Wang, B.; Gai, J.; Chen, J.; Yang, F.; Cao, Y.; Li, H.; Kang, J.; Xiang M. *J. Appl. Polym. Sci.* **2014**, *131*, 40027.
13. Kang, J.; Peng, H.; Wang, B.; Chen, Z.; Li, J.; Chen, J.; Cao, Y.; Li, H.; Yang, F.; Xiang, M. *J. Appl. Polym. Sci.* **2014**, *131*, 40015.
14. Dorset, D. L.; McCourt, M. P.; Kopp, S.; Schumacher, M.; Okihara, T.; Lotz. B. *Polymer* **1998**, *39*, 6331.
15. Brckner, S.; Phillips, P. J.; Mezghani, K.; Meille. S. V. *Macromol. Rapid Commun.* **1997**, *18*, 1.
16. Bruckner, S.; Meille, S. V.; Petraccone, V.; Pirozzi, B. *Prog. Polym. Sci.* **1991**, *16*, 361.
17. Lotz, B.; Graff, S.; Straupe, C.; Wittmann, J. C. *Polymer* **1991**, *32*, 2902.
18. Hoffman, J.; Davis, G. T.; Lauritzen, J., Jr. In Treatise on Solid State Chemistry; Hannay, N. B., Ed.; Springer: US, **1976**, p 497.
19. Meille, S. V.; Bruckner, S.; Porzio, W. *Macromolecules* **1990**, *23*, 4114.
20. Turner-Jones, A.; Cobbold, A. J. *J. Polym. Sci. Part B: Polym. Lett.* **1968**, *6*, 539.

21. Morrow, D. R.; Newman, B. A. *J. Appl. Phys.* **1968**, *39*, 4944.
22. Zhang, Y. F.; Xin, Z. *J. Appl. Polym. Sci.* **2006**, *100*, 4868.
23. Liu, D.; Kang, J.; Xiang, M.; Cao, Y. *J. Polym. Res.* **2013**, *26*, 126.
24. Kang, J.; Xiong, B.; Liu, D.; Cao, Y.; Chen, J.; Yang, F.; Xiang, M. *J. Polym. Res.* **2014**, *21*, 485.
25. Kang, J.; Wang, B.; Peng, H.; Li, J.; Chen, J.; Gai, J.; Cao, Y.; Li, H.; Yang, F.; Xiang, M. *Polym. Adv. Technol.* **2014**, *25*, 97.
26. Lu, Q.; Dou, Q. *J. Polym. Res.* **2009**, *16*, 555.
27. Na, B.; Li, Z.; Lv, R.; Tian, N.; Zou, S. *J. Polym. Res.* **2011**, *18*, 2103.
28. Libster, D.; Aserin, A.; Garti, N. *Polym. Adv. Technol.* **2007**, *18*, 685.
29. Ni, Q.; Zhu, X.; Wang, Y.; Liu, Z. *J. Polym. Res.* **2011**, *18*, 917.
30. Li, J.; Wang, S. W.; Zhan, K. J.; Yang, W.; Xie, B. H.; Yang, M. B. *J. Appl. Polym. Sci.* **2012**, *124*, 993.
31. Pawlak, A.; Piorkowska, E. *Colloid Polym Sci* **2001**, *279*, 939.
32. Zhang, B.; Chen, J.; Ji, F.; Zhang, X.; Zheng, G.; Shen, C. *Polymer* **2012**, *53*, 1791.
33. Li, H.; Sun, X.; Yan, S.; Schultz, J. M. *Macromolecules* **2008**, *41*, 5062.
34. Li, H.; Yan, S. *Macromolecules* **2011**, *44*, 417.
35. Li, H.; Jiang, S.; Wang, J.; Wang, D.; Yan, S. *Macromolecules* **2003**, *36*, 2802.
36. Lotz, B.; Wittmann, J. C.; Lovinger, A. J. *Polymer* **1996**, *37*, 4979.
37. Dimeska, A.; Phillips, P. J. *Polymer* **2006**, *47*, 5445.
38. Mezghani, K.; Phillips, P. J. *Polymer* **1998**, *39*, 3735.
39. Zhao, S. Xin, Z. *J. Polym. Sci. Part B: Polym. Phys.* **2010**, *48*, 653.
40. Reyes-de-Vaaben, S.; Aguilar, A.; Avalos, F.; Ramos-de Valle, L. F. *J. Therm. Anal. Calorim.* **2008**, *93*, 947.
41. Zhang, Y. F. *J. Macromol. Sci. Part B* **2008**, *47*, 891.
42. Zhang, Y. F.; Xin, Z. *J. Polym. Sci. Part B: Polym. Phys.* **2007**, *45*, 590.
43. Bai, H.; Wang, Y.; Liu, L.; Zhang, J.; Han, L. *J. Polym. Sci. Part B: Polym. Phys.* **2008**, *46*, 1853.
44. Bai, H.; Wang, Y.; Zhang, Q.; Liu, L.; Zhou, Z. *J. Appl. Polym. Sci.* **2009**, *111*, 1624.
45. Lorenzo, A. T.; Muller, A. J. *J. Polym. Sci. Part B: Polym. Phys.* **2008**, *46*, 1478.
46. Su, F.; Li, X.; Zhou, W.; Zhu, S.; Ji, Y.; Wang, Z.; Qi, Z.; Li, L. *Macromolecules* **2013**, *46*, 7399.
47. Li, X.; Su, F.; Ji, Y.; Tian, N.; Lu, J.; Wang, Z.; Qi, Z.; Li, L. *Soft Matter* **2013**, *9*, 8579.
48. Cavallo, D.; Gardella, L.; Portale, G.; Muller, A. J.; Alfonso, G. C. *Polymer* **2014**, *55*, 137.
49. Fillon, B.; Wittmann, J. C.; Lotz, B.; Thierry, A. *J. Polym. Sci. Part B: Polym. Phys.* **1993**, *31*, 1383.
50. Fillon, B.; Thierry, A.; Wittmann, J. C.; Lotz, B. *J. Polym. Sci. Part B: Polym. Phys.* **1993**, *31*, 1407.
51. Fillon, B.; Lotz, B.; Thierry, A.; Wittmann, J. C. *J. Polym. Sci. Part B: Polym. Phys.* **1993**, *31*, 1395.
52. Lorenzo, A. T.; Arnal, M. L.; Sánchez, J. J.; Muller, A. J. *J. Polym. Sci. Part B: Polym. Phys.* **2006**, *44*, 1738.
53. Muller, A. J.; Hernandez, Z. H.; Arnal, M. L.; Sanchez, J. J. *Polym. Bull.* **1997**, *39*, 465.
54. Liu, Q.; Sun, X.; Li, H.; Yan, S. *Polymer* **2013**, *54*, 4404.
55. Azzurri, F.; Alfonso, G. C. *Macromolecules* **2005**, *38*, 1723.
56. Cavallo, D.; Azzurri, F.; Balzano, L.; Funari, S. r. S.; Alfonso, G. C. *Macromolecules* **2010**, *43*, 9394.
57. Azzurri, F.; Alfonso, G. C. *Macromolecules* **2008**, *41*, 1377.
58. Zhang, B.; Chen, J.; Cui, J.; Zhang, H.; Ji, F.; Zheng, G.; Heck, B.; Reiter, G.; Shen, C. *Macromolecules* **2012**, *45*, 8933.
59. Kang, J.; Weng, G.; Chen, Z.; Chen, J.; Cao, Y.; Yang, F.; Xiang, M. *RSC Adv.* **2014**, *4*, 29514.
60. Kang, J.; Chen, Z.; Zhou, T.; Yang, F.; Chen, J.; Cao, Y.; Xiang, M. *J. Polym. Res.* **2014**, *21*, 384.
61. Varga, J.; Menyhard, A. *Macromolecules* **2007**, *40*, 2422.
62. Luo, F.; Geng, C.; Wang, K.; Deng, H.; Feng, C.; Fu, Q.; Na, B. *Macromolecules* **2009**, *42*, 9325.
63. Yamamoto, Y.; Inoue, Y.; Onai, T.; Doshu, C.; Takahashi, H.; Uehara, H. *Macromolecules* **2007**, *40*, 2745.
64. Marco, C.; Gomez, M. A.; Ellis, G.; Arribas, J. M. *J. Appl. Polym. Sci.* **2002**, *84*, 1669.
65. Muller, A. J.; Arnal, M. L. *Prog. Polym. Sci.* **2005**, *30*, 559.
66. Kotek, J.; Kelnar, I.; Baldrian, J.; Raab, M. *Eur. Polym. J.* **2004**, *40*, 679.
67. Scudla, J.; Raab, M.; Eichhorn, K. J.; Strachota, A. *Polymer* **2003**, *44*, 4655.
68. Li, J. X.; Cheung, W. L.; Chan, C. M. *Polymer* **1999**, *40*, 2089.
69. Liu, Q.; Dou, Q. *J. Polym. Res.* **2009**, *16*, 555.
70. Ali, D.; Tuncer, Y. *J. Polym. Res.* **2009**, *16*, 489.